



Experimental and Numerical Study of the Heat Transfer Characteristics of Aluminium Metal Foam (with/without channels) Subjected to Steady Water Flow

Bayomy, A. M.* and Saghir, M. Z.

Department of Mechanical and Industrial Engineering, Ryerson University, 350 Victoria St, Toronto, ON, Canada

ABSTRACT

Rapid developments in the design of chips and electronic devices for high-performance computers have necessitated new and more effective methods of chip cooling. The purpose of this study was to investigate the heat transfer characteristics of aluminium foam heat sink for the Intel core i7 processor. Three aluminium foam heat sink models were used in the study: without channels (A), with two channels (B), and with three channels (C). The aluminium foam heat sink was subjected to a steady flow of water covering the non-Darcy flow regime (541 to 1353 Reynolds numbers). The bottom side of the heat sink was heated with a heat flux between 8.5 and 13.8 W/cm². The distributions of the local surface temperature and the local Nusselt number were measured and compared with numerical data obtained using the finite element method for all three models. The average Nusselt number was obtained for the specified range of Reynolds numbers, and an empirical correlation of the average Nusselt number as a function of the Reynolds number was derived for each model. The results revealed that the local surface temperature increases as the heat flux increases, decreasing the Reynolds number and increasing the flow direction axis for all three models. Model (A) achieved a lower local temperature than models (B) and (C). Compared with model (A), models (B) and (C) reduced the average Nusselt number by 10% and 25%, respectively. The pressure drop across the foam was also measured. The thermal efficiency index was defined in this study in order to obtain the optimal design condition for the aluminium foam heat sink models. The results revealed that the optimum design condition is model (B) at Re=1353. The numerical results were in good agreement with the local Nusselt number and the local experimental temperature with a maximum relative error of 3% and 2% respectively.

Keywords: Electronic cooling, forced convection, porous media, heat transfer, heat sink, metal foam

Article history:

Received: 08 January 2016

Accepted: 11 November 2016

E-mail addresses:

ayman.bayomy@ryerson.ca (Bayomy, A. M.),

zsaghir@ryerson.ca (Saghir, M. Z.),

*Corresponding Author

INTRODUCTION

Electronic components depend on electrical currents passing through resistance. This is accompanied by heat flux dissipation. The rapid developments in the design of electronic chips have resulted in an increase in the amount of heat generated per unit of volume. The international technology road map for semiconductors reported that the heat flux of chips rose by 200 W/cm² (Lee, 2009). Conventional convective cooling methods are only capable of removing small amounts of heat flux, making it important to search for new methods of cooling high-speed electronic components. The performance reliability and lifetime of electronic components are inversely related to the temperature of the component. In silicon semi-conductor devices, reductions in temperature increase their performance reliability and lifetime. Gochman et al. (2003) reported that the heat dissipation of desktop and mobile processors are 100W and 30W respectively.

In order to enhance the heat transfer rate of modern high speed electronic devices, researchers have conducted extensive investigations using different shapes and arrangements (single or multiple square, rectangular and circular modules (rods)) mounted on the heated surface in order to increase the surface to volume ratio of heat sinks (Buller & Kilburn, 1981; Sparrow, Niethammer, & Chaboki, 1982; Sparrow, Yanezmoreno, & Otis, 1984; Jubran, Swiety, & Hamdan, 1996; Iwasaki & Ishizuka, 2000; Igarashi, Nakamura, & Fukuoka, 2004)

Many studies have been conducted using various types of heat sinks for electronic cooling, either extending the surface area or increasing the fluid flow. Despite this research, there still exists a demand for more effective electronic cooling methods.

The use of porous media as a heat sink subjected to forced cooling fluid is a new technique used to enhance heat transfer from the surface of electronics. Metal foam is a porous material with a low density and novel thermal, electrical, mechanical and acoustic properties. This material provides good heat transfer due to its large surface area to volume ratio (roughly 1000-3000 m²/m³) (Zhao, 2012). The heat transfer characteristics of metal foam are directly affected by microstructural properties such as porosity, relative density, pore density, pore size, ligament diameter and permeability (Hwang, Hwang, Yeh, and Chao, 2002; Zhao, Kim, and Hodson, 2004; Lu, Zhao, and Tassou, 2006 ; Seyf and Layeghi, 2010; Mancin, Zilio, Diani, and Rossetto, 2012).

The effective thermal conductivity of ERG aluminium foams was studied by Boomsma and Poulikakos (2001). They demonstrated that in high porosity foam, the solid phase thermal conductivity controls the overall effective thermal conductivity of the aluminium foam. Boomsma and Poulikakos (2001) also derived an expression of effective thermal conductivity. In addition, Zhao, Lu, & Tassou (2006) and Klett et al. (2001) observed that the metal foam heat exchanger achieves higher heat transfer than the conventional finned tube heat exchanger. Studies have also been conducted on the effects of using metal foam (Sung, Kim, and Hyun, 1995; Fu, Leong, Huang, and Liu, 2001; Rachedi and Chikh, 2001; Mahajan & Bhattachatya, 2002; Nield, Kuznetsov, and Xiong, 2003; Kim, Paek, and Kang, 2003; Tzeng, Jeng, and Wang, 2006; Hooman and Ejlali, 2007a; Hooman and Haji-Sheikh, 2007b; Bai and Chung, 2011; Ding, Lu, Chen, He, & Ou, 2011) which demonstrated the positive effect caused by employing the metal foam.

A small number of studies have used water as a working coolant fluid through metal foams. Boomsma, Poulikakos, and Zwick (2003) conducted an experimental comparison of the thermal resistance of a compressed metal foam heat exchanger and commercially available heat exchangers using water as a coolant. They found that the thermal resistance of the compressed foam heat exchanger is two to three times lower than that of other heat exchangers. Noh, Lee, and Lee (2006) conducted an experimental study of a non-Darcy water flow in an annulus filled with high porosity aluminium foam and presented the correlations of the average Nusselt number and friction factor. Hetsroni, Gurevich, and Rozenblit (2005) conducted an experimental study of the transmission window cooling technique of an accelerator using aluminium foam. Dukhan, Bağcı, and özdemir (2015) conducted an experimental study of thermal development in open cell metal foam subjected to a constant heat flux. The flow rates used covered both the Darcy and non-Darcy regimes.

This paper presents an experimental and numerical study of aluminium foam models used as heat sinks in the cooling of an Intel core i7 processor (electronic cooling). Three aluminium foam heat sink models were used in the study: without channels (A), with two channels (B), and with three channels (C). The aluminium foam was subjected to a water flow covering the non-Darcy flow regime. Local temperature distributions were measured for different heat fluxes and Reynolds numbers and the local Nusselt number was calculated based on the local surface temperature of each heat sink model. The average Nusselt number was obtained for the entire range of Reynolds numbers. An empirical correlation of the average Nusselt number was developed based on the Reynolds number of each model. The pressure drop across each heat sink model was also measured and the thermal performance of the aluminium foam heat sink was evaluated based on the average Nusselt number and the pumping power required for each model. The thermal efficiency index was defined in order to obtain the optimum design condition for the use of aluminium foam as a heat sink. Lastly, a numerical approach was used (finite element method) (COMSOL Multiphysics, 2015) and the results were compared with those obtained experimentally.

EXPERIMENTAL APPARATUS AND PROCEDURES

An experimental setup was developed in order to examine the heat transfer characteristics of aluminium foam (with and without channels) as a heat sink in the cooling of an Intel core i7 processor.

Test Section and Experimental Facility

The experimental setup was developed before by Bayomy, Saghir, and Yousife (2016). It consisted of a pump with a control valve, a tank, flow meter and pressure transducer (see Figure 1). The flow meter range was from 0 to 3 gpm with corresponding output signals between 4 and 20 mA.

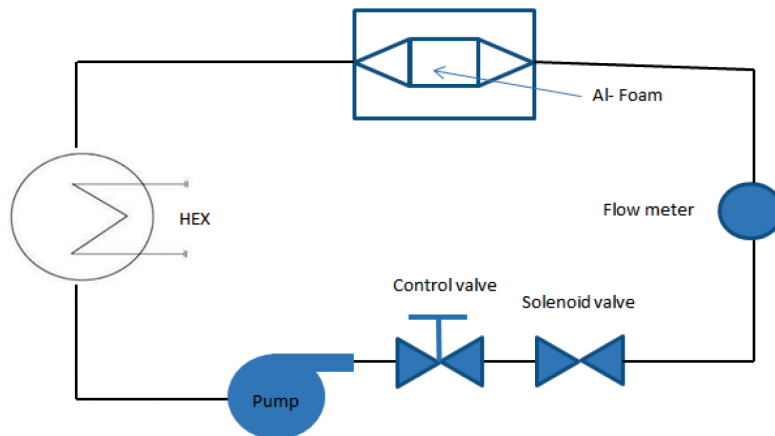


Figure 1. Experimental schematic diagram (Bayomy et al. 2016)

The pressure differential transducer range was from 0 to 30 psi with corresponding output signals between 0 and 10 vdc. The test section consisted of high temperature Teflon insulation attached to a 37.5mm 37.5mm heater (corresponding to the size of an Intel core i7 processor).

The heater contained an adjustable current input in order to control the heat flux, as shown in Figure 2. Eight type (T) thermocouples were attached to the surface of the heater to measure the surface temperature and two thermocouples were used to measure the inlet and outlet water temperatures. The positioning of the thermocouples can be seen in Figure 3(a). Because of their large head connections, the thermocouples were inserted through the Teflon insulation in a staggered arrangement, as shown in Figure 3(b).



Figure 2. Test section heater (Bayomy et al. 2016)

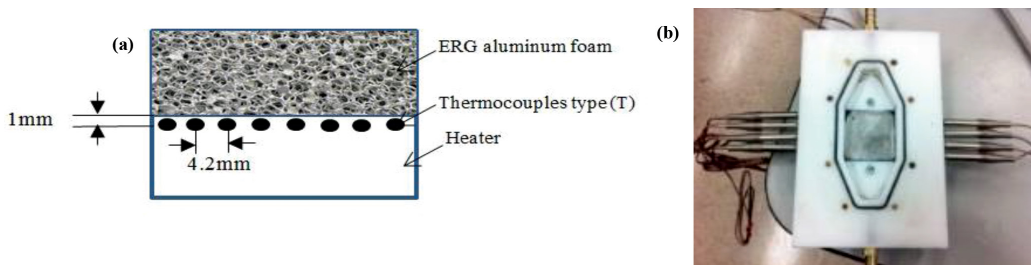


Figure 3. Thermocouples positions and arrangements (Bayomy et al. 2016)

All of the signals from the thermocouples, the flow metre and the pressure transducer were connected to a data acquisition system in order to monitor and save the experimental data. The ERG aluminium metal foam (alloy 6101-T6) was cut to match the size of the heater (37.5mm37.5mm). Three aluminium foam heat sink models were used in the study: one without channels (A), one with two channels (B) and one with three channels (C), as shown in Figure 4. The dimensions of the channels for models (B) and (C) are shown in Figure 5. The physical and geometric properties of the ERG test section foam are as follows: relative density (ρ_r) of 9%, pore density of 40PPI, permeability (K) of $3.38e-8 \text{ m}^2$, porosity (ϵ) of 0.9 and thermal conductivity of solid material (K_s) of 218 W/m.K . It is important to note that these properties are not all independent of one another. The relationships between them are presented by Calmidi and Mahajan (2000).

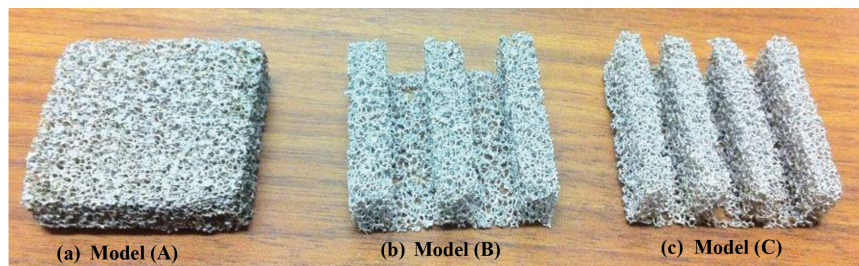


Figure 4. ERG aluminium foam models

The Plexiglas cover has two openings, just before and after the aluminium foam, to allow for connections to the pressure differential transducer ports, as shown in Figure 6. In order to obtain experimental steady state conditions, the surface temperature, inlet and outlet temperatures, pressure drop across the foam, and water flow rate were monitored using the data acquisition system.

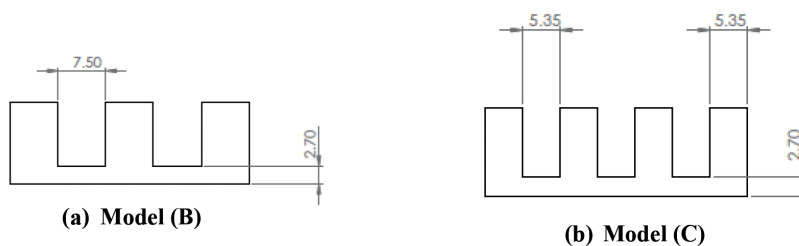


Figure 5. Models B & C dimensions



Figure 6. Test section (Bayomy et al. 2016)

Uncertainty Analysis

The uncertainties of the temperature, flow rate and pressure drop were 0.75% (°C), 0.44% (gpm) and 0.03% (psi), respectively. These values were obtained from the calibration process for each instrument based on slandered and random error. The uncertainties of (Nu_x) and (Re) were obtained using the Taylor method (Taylor, 1995). If x, y, z measure quantities such as temperature, flow rate and pressure difference, and those measurement quantities have uncertainties of $\delta x, \delta y, \delta z$ and are used to calculate parameters such as the local Nusselt number $Nu_x(x, y, z)$, then the uncertainty of the local Nusselt number is:

$$\delta Nu_x = \sqrt{\left(\frac{\partial Nu_x}{\partial x} \cdot \delta x\right)^2 + \dots + \left(\frac{\partial Nu_x}{\partial y} \cdot \delta y\right)^2 + \dots + \left(\frac{\partial Nu_x}{\partial z} \cdot \delta z\right)^2} \quad (1)$$

The local Nusselt number and the Reynolds number are calculated as follows:

$$h_x = \frac{q''}{(T_x - T_{in})} \quad (2)$$

$$Nu_x = \frac{h_x D_e}{k_{eff}} \quad (3)$$

$$Re = \frac{U \cdot D_e}{\nu_f} \quad (4)$$

Where h_x represents the local heat transfer coefficient over the heater surface, T_x represents the local surface temperature, T_{in} represents the inlet water temperature, D_e represents the hydraulic diameter of the channel, U represents the water velocity throughout the test section, ν_f represents the kinematic viscosity of the fluid, and represents the effective thermal conductivity of the metal foam filled with water.

The maximum value of the uncertainty of the local Nusselt number was $\pm 2.4\%$ and the uncertainty of the Reynolds number was $\pm 0.44\%$. The energy balance was checked by comparing the quantity of heat absorbed by the water with the actual heat input of the heater. The heat loss was obtained by subtracting the actual heat input from the quantity of heat absorbed by the water. The result was 0.2% heat loss.

NUMERICAL MODEL DESCRIPTION

Numerical results were obtained using the finite element technique in order to allow for a comparison with the experimental results.

Governing Equations

It is important to state the assumptions upon which the equations are based prior to the formulation of the model. Those assumptions are:

1. The fluid passing through the channel is Newtonian and incompressible.
2. The porous medium is homogenous and has a uniform porosity.

3. Local thermal equilibrium between the fluid and the solid phase of metal foam.
4. No heat generation occurs inside the porous medium.
5. Variation in the thermo-physical properties of the solid phase can be neglected.

The set of governing equation were solved based on the numerical model assumptions. These governing equation consists of the Brinkman- Forchheimer equation and energy equation which describe the fluid flow and heat transfer inside porous media respectively, as follows:

$$\frac{\rho}{\epsilon} \left((\mathbf{U} \cdot \nabla) \frac{\mathbf{U}}{\epsilon} \right) = \nabla \cdot (-p\mathbf{I} + \frac{\mu}{\epsilon} (\nabla \mathbf{U} + (\nabla \mathbf{U})^T)) - \left(\frac{\mu}{K} + \beta_f |\mathbf{U}| \right) \mathbf{U} + \mathbf{F} \quad (5)$$

$$\nabla \cdot (\rho \mathbf{U}) = 0 \quad (6)$$

$$\rho c_p \mathbf{U} \cdot \nabla T = \nabla \cdot (k_{\text{eff}} \cdot \nabla T) \quad (7)$$

Where ρ represents the water density, c_p represents the water specific heat, ϵ represents the porosity of the aluminium metal foam, p represents the pressure, \mathbf{U} represents the velocity field vector, β_f represents the Forchheimer coefficient, T represents the temperature, μ represents the dynamic viscosity of water, K represents the permeability of the aluminium foam and k_{eff} represents the effective thermal conductivity of the aluminium metal foam when filled with water. The effective thermal conductivity of the porous medium filled with fluid can be described by the porosity (ϵ) and thermal conductivities of the solid phase (k_s) and fluid phase (k_f) (Kaviany, 1995) using the following equation:

$$k_{\text{eff}} = \epsilon \cdot k_f + (1 - \epsilon) \cdot k_s \quad (8)$$

However, an accurate representation of the structural parameters of the metal foam is important for the estimation of effective thermal conductivity. Calmidi and Mahajan (1999) obtained the effective thermal conductivity of ERG aluminium foam based on one-dimensional heat conduction through two-dimensional foam structures. Boomsma and Pouliakos (2001) extended the previous research by investigating a three-dimensional analytical model of effective thermal conductivity of ERG foams. This model was used to evaluate the effective thermal conductivity of the ERG aluminium foam (alloy 6101-T6) used in the present study.

Boundary Conditions

The boundary conditions can be concluded as an inlet temperature and velocity (assuming a flat profile), at the inlet portion, open boundary at the outlet portion, heat flux from the bottom of the heater and adiabatic walls at the remainder of the surface (see Figure 7).

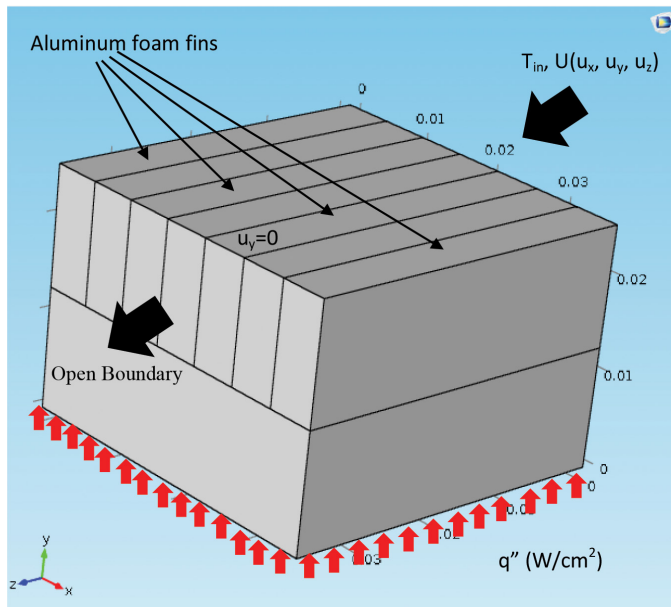


Figure 7. Boundary conditions

Mesh Sensitivity Analysis

A tetrahedral element was used to describe the numerical model. In order to perform mesh sensitivity analysis, calculations of the maximum temperature and local Nusselt number was performed for different numbers of domain elements, as shown in Figure 8. The number of elements used was 1847400 and the variation was less than 0.001, as shown in Figure 9. At every time step, the finite element technique obtained the errors in all independent parameters such as U, P, and T as follows:

$$R = \frac{1}{n.m} \sum_{i=1}^m \sum_{j=1}^n \left| \frac{(F_{i,j}^{s+1} - F_{i,j}^s)}{F_{i,j}^{s+1}} \right| \quad (9)$$

Where F represents one of the independent parameters, s represents the number of iterations, and (i, j) represent the x and y coordinates. The solution reached convergence when R was below 1×10^{-6} for each independent parameter.

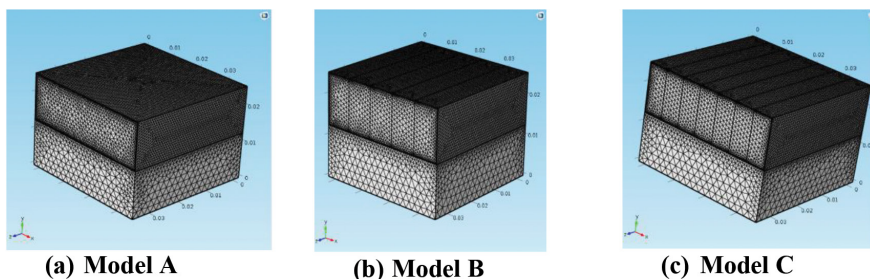


Figure 8. Finite element model

Heat Transfer Characteristics of AMF

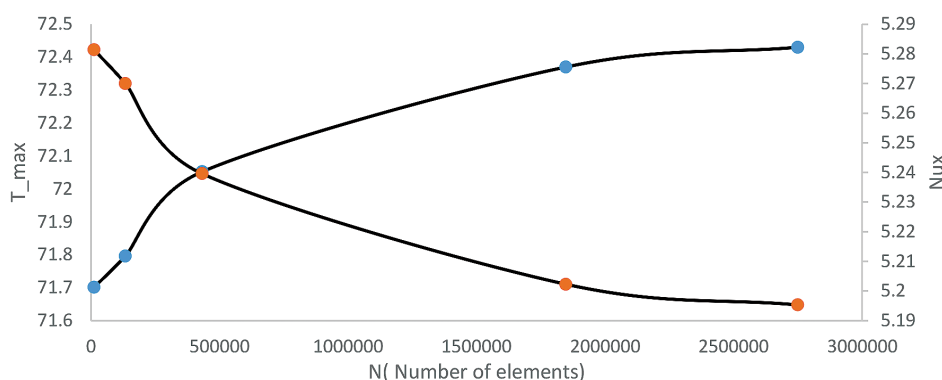


Figure 9. Mesh independent

RESULTS AND DISCUSSION

In this experimental study, three aluminium foam heat sink models (A, B, and C) were subjected to a uniform heat flux ranging from 13.8 to 8.5 W/cm². The water flow covered the Forchheimer regime (non-Darcy regime). In addition, a numerical model was developed using the finite element technique and the numerical results compared with the experimental results.

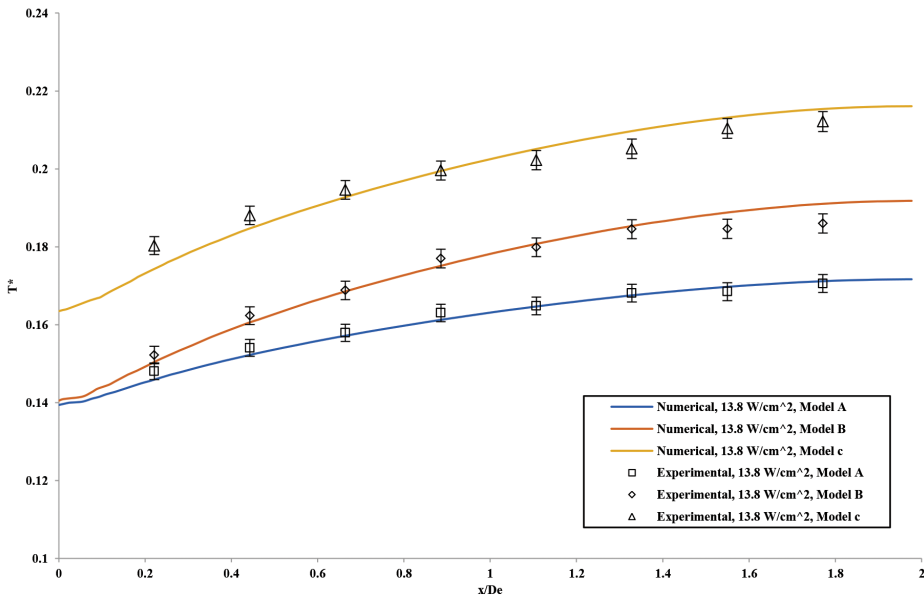
Local Dimensionless Temperature Distributions Over the Surface

Figures 10(a, b) illustrate the surface temperature distributions along the dimensionless flow direction axis (x/De) at $q'' = 13.8$ and 10.6 W/cm² respectively, and $Re = 1353$ for models (A), (B) and (C). As we can see, the surface temperature showed an increase in the flow direction. This trend was observed in previous experimental studies (Fu et al., 2001; Noh et al., 2006). The results revealed that model (A) achieved a lower temperature distribution when compared with models (B) and (C). The results also revealed that the dimensionless local surface temperatures of models (A) and (B) were almost identical at the beginning of the channel ($x/De = 0 - 0.3$) and began to diverge from each other along with the axial flow direction distant. The same trend can be observed in Figure 11(a, b) which illustrates the temperature distributions at $Re = 902$ and $q'' = 13.8$ and 8.5 W/cm² respectively. Figure 12 shows the temperature distributions at $Re = 541$ and $q'' = 13.8$ W/cm². We can also see that the surface temperature increases along with decreases in the Reynolds number and increases in the heat flux.

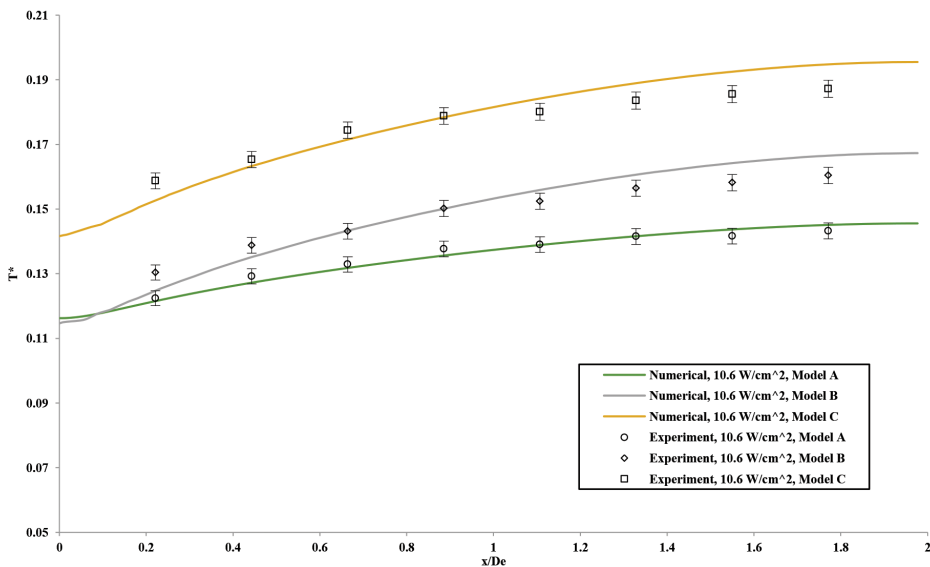
In order to complement the experimental results, a numerical model was developed using the finite element technique. Figures 10, 11 and 12 show the experimental and numerical surface temperature results for different heat flux and Reynolds numbers ($Re = 1353, 902$ and 541). The numerical results are in good agreement with the experimental results, with a maximum relative error of 2%.

In addition, Figures 13 and 14 show the temperature contours of each model at $q'' = 13.8$ W/cm² and $Re = 1353$ and 902 respectively. The results revealed that the temperature of the heated surface (electronic surface) increases along with the flow direction axis. In addition, the use of channels in the aluminium foam (models B and C) creates a non-uniform temperature

distribution along the line which is perpendicular to the flow direction. As shown in Figure 15, the temperature distribution along the line perpendicular to the flow direction of model (A) is perfectly uniform and lower than that of models (B) and (C) which suffer from non-uniform temperature.



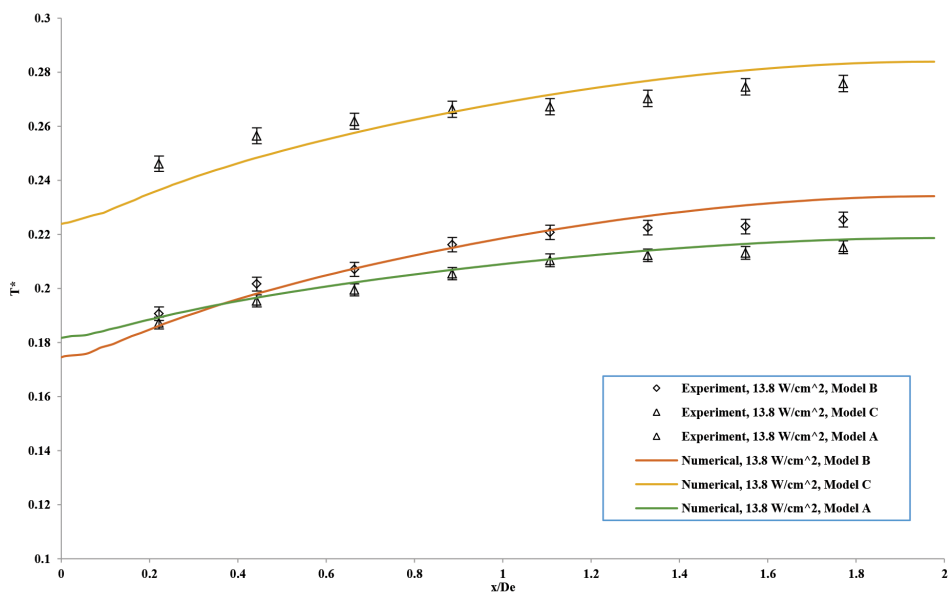
(a) Temperature distributions at $q'' = 13.8 \text{ W/cm}^2$



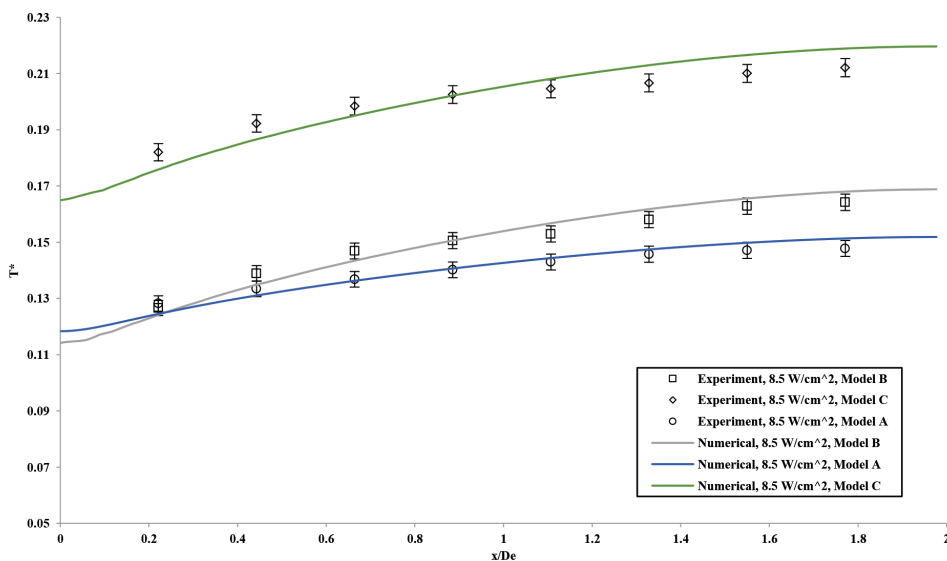
(b) Temperature distributions at $q'' = 10.6 \text{ W/cm}^2$

Figure 10. Surface temperature distributions at $Re = 1353$

Heat Transfer Characteristics of AMF



(a) Temperature distributions at $q'' = 13.8 \text{ W/cm}^2$



(b) Temperature distributions at $q'' = 8.5 \text{ W/cm}^2$

Figure 11. Surface temperature distributions at $Re = 902$

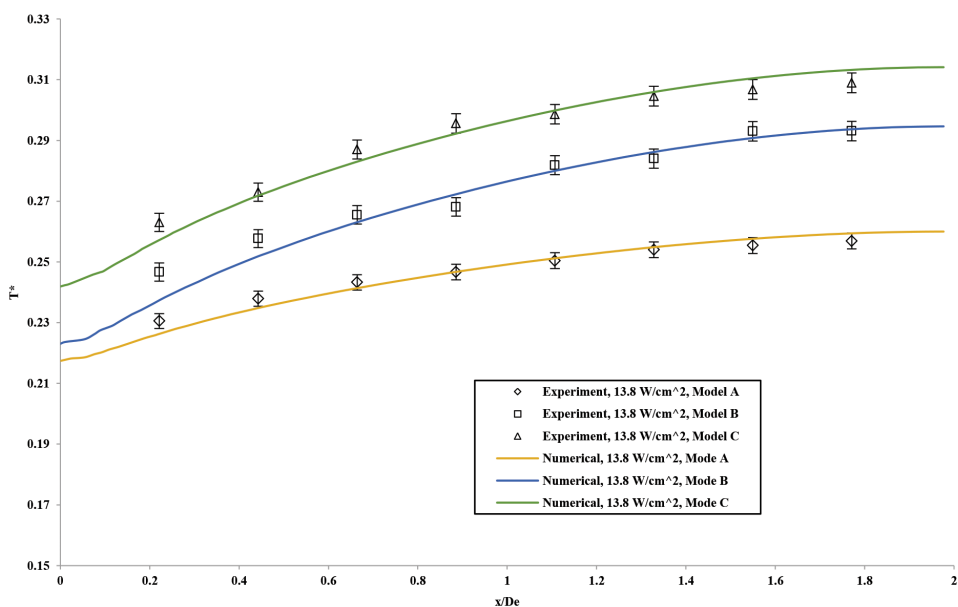


Figure 12. Surface temperature distributions at Re= 541

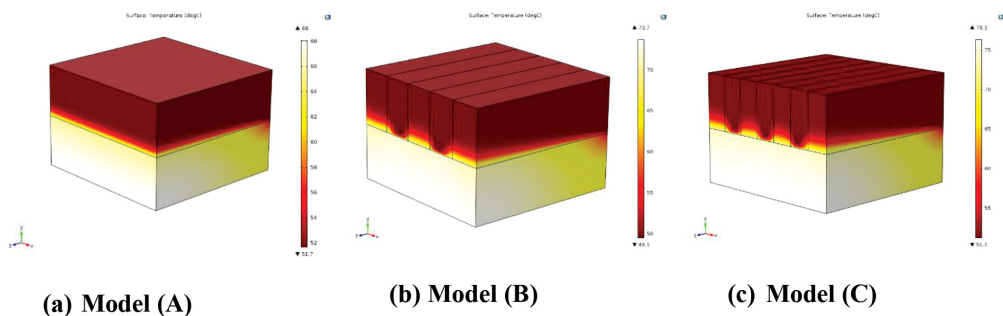


Figure 13. Temperature contours at $q''=13.8 \text{ W/cm}^2$ and Re=1353

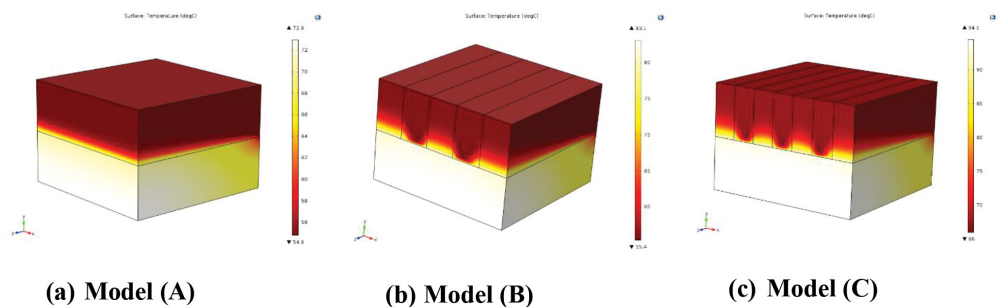


Figure 14. Temperature contours at $q''=13.8 \text{ W/cm}^2$ and Re=902

Heat Transfer Characteristics of AMF

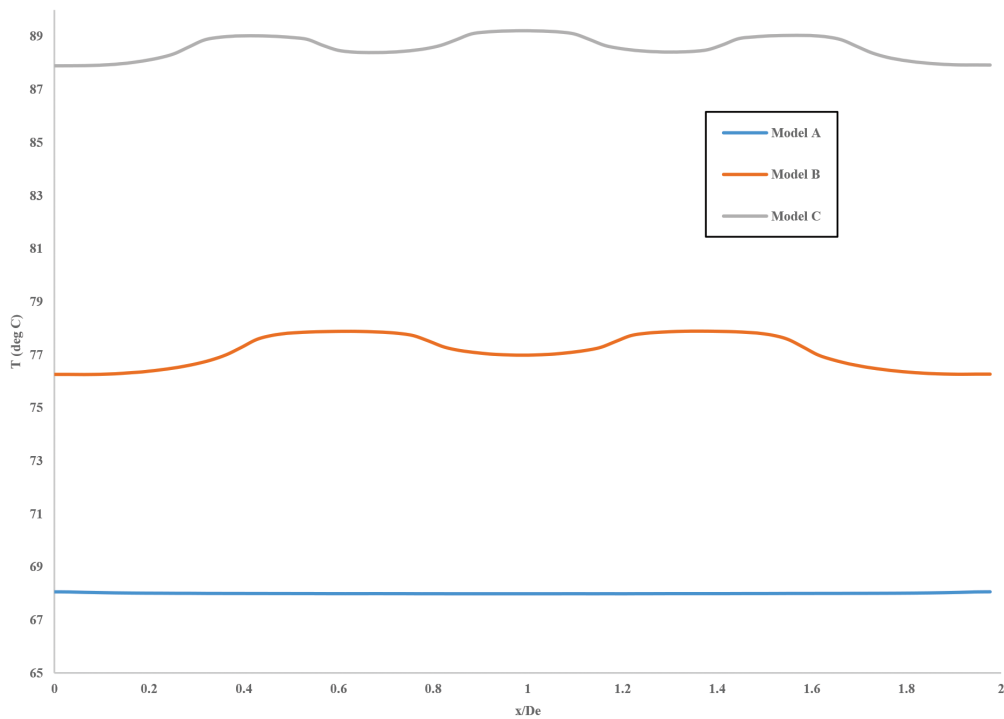
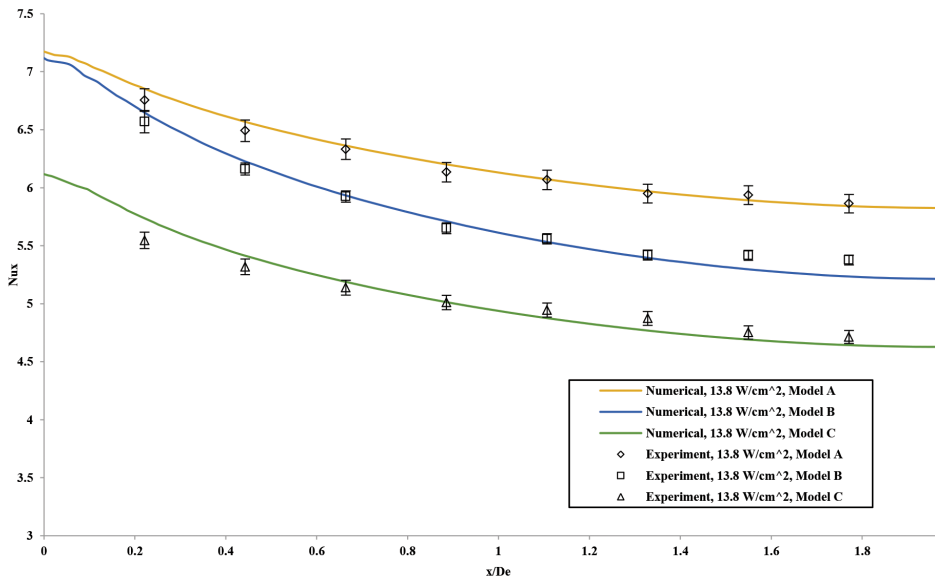


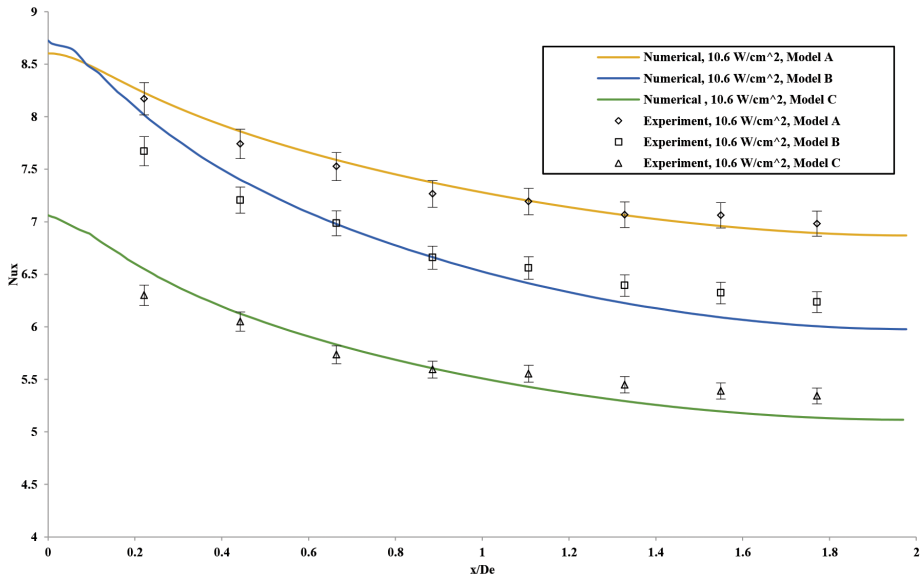
Figure 15. Temperature distribution at $q'' = 13.8 \text{ W/cm}^2$ and $Re=902$

Local and Average Nusselt Number Distributions

Figures 16 and 17 show the calculated local Nusselt number variation with the dimensionless flow direction axis at $Re= 1353$ and 902 respectively. As we can see, the local Nusselt number is high in the entry region and begins to decrease until a constant value is reached when the flow and temperatures become thermally fully developed. This means that in the entry regions, the local Nusselt number is inversely proportional to the boundary layer thickness. The results revealed that the Nusselt number was higher for model (A) compared with models (B) and (C). The numerical results were in good agreement with the experimental results with a maximum relative error of 3%.



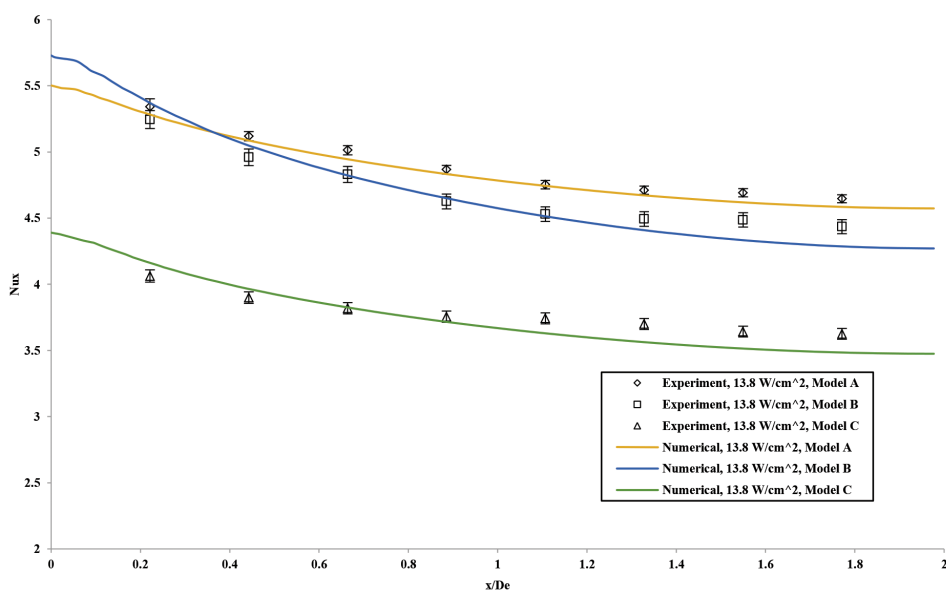
(a) Nusselt number distributions at $q'' = 13.8 \text{ W/cm}^2$



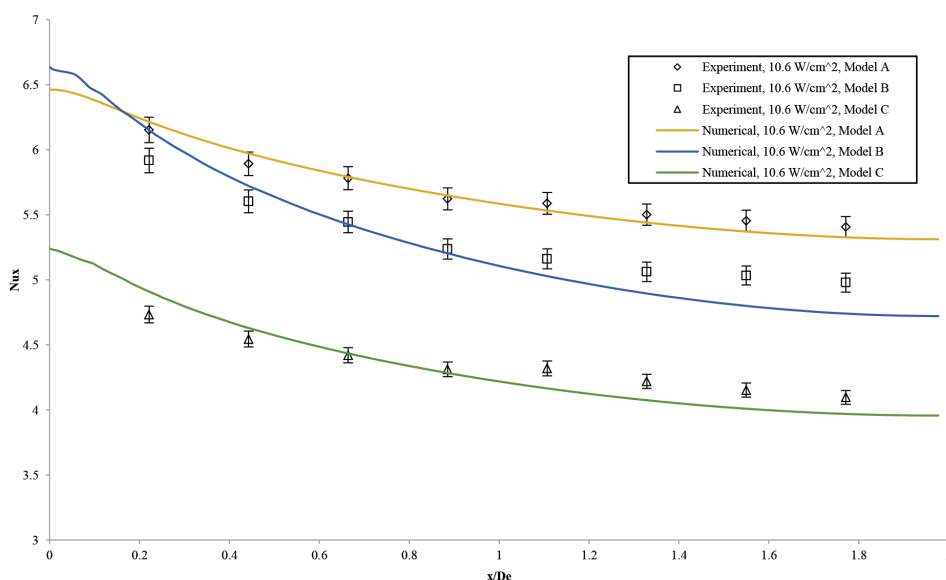
(b) Nusselt number distributions at $q'' = 10.6 \text{ W/cm}^2$

Figure 16. Experimental and numerical results of Nusselt number at $Re=1353$

Heat Transfer Characteristics of AMF



(a) Nusselt number distributions at $q'' = 13.8 \text{ W/cm}^2$



(b) Nusselt number distributions at $q'' = 10.6 \text{ W/cm}^2$

Figure 17. Experimental and numerical results of Nusselt number at $Re=902$

In order to determine the heat transfer performance of aluminium foam models used as a heat sink, the average Nusselt number was obtained using the following equation:

$$Nu_{,avg} = \frac{1}{L} \int_0^L Nu_x \, dx \quad (16)$$

Where L represents the channel length and Nu_x represents the local Nusselt number. Figure 18 shows the relationship between the average Nusselt number of models (A), (B) and (C) and the Reynolds number. This figure clearly illustrates that the average Nusselt number increases with increase in the Reynolds number for different models. The results also revealed that the average Nusselt number was higher for model (A) compared with models (B) and (C).

The relationship between the average Nusselt number and the Reynolds number was obtained using the following equation:

$$Nu_{avg} = CRe^m \tag{17}$$

Where C and m are constants listed in Table 1 and obtained using the present experimental data of steady water flow through different aluminium foam heat sink models for a given range of Reynolds numbers (Forchheimer regime).

Table 1
Average Nusselt Number Constants

Heat Sink Models	C	m
Model (A)	0.342	0.41
Model (B)	0.121	0.54
Model (c)	0.1	0.56

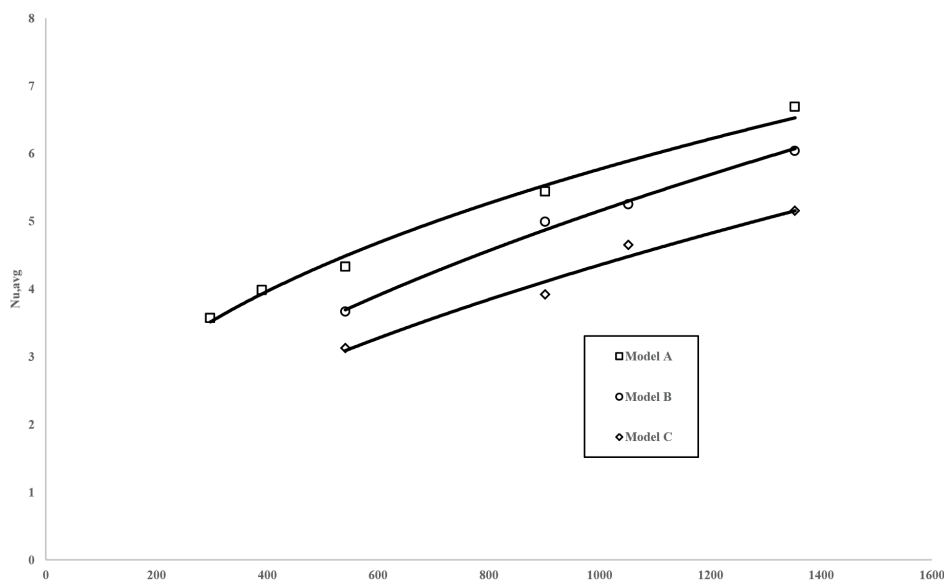


Figure 18. Average Nusselt number versus Reynolds number

As shown in Figure 19, the ratio between the average Nusselt number of model (B) ($Nu_{avg,B}$) and model (A) ($Nu_{avg,A}$) is about 0.9 and the ratio between the average Nusselt number of model (C) ($Nu_{avg,C}$) and model (A) ($Nu_{avg,A}$) is about 0.75. This means that model (B) and model (C) reduced the heat transfer by 10% and 25% respectively.

Introducing channels in the heat sink (models B and C) is supposed to increase the surface area to volume ratio, causing increases in the heat transfer rate. This is in direct contrast to the results obtained in the experiment which revealed that models (B) and (C) reduced the heat transfer rate by 10% and 25%, respectively. The velocity contours obtained from the finite element will explain this phenomenon.

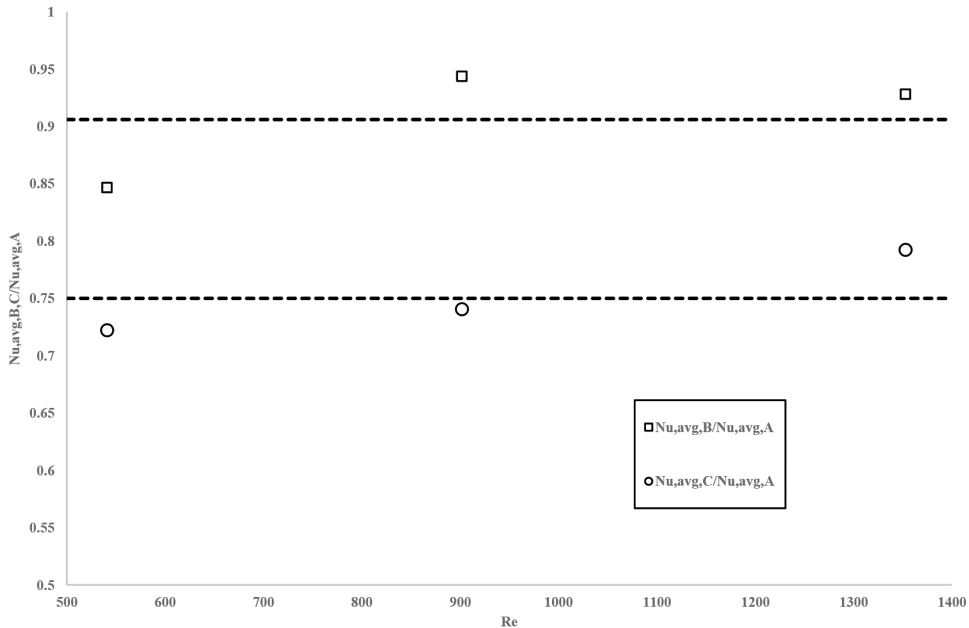


Figure 19. Average Nusselt number ratio of model (B) and (C) to model (A)

Figures 20 and 21 show the velocity contours for models (A), (B) and (C) at $q''=13.8 \text{ W/cm}^2$ and $Re=1353$ and 902 respectively. The results revealed that model (A) has a uniform velocity throughout the aluminium foam heat sink. On the other hand, the velocity contours of models (B) and (C) are different due to the acceleration of the flow inside the channels and a reduction of the water flow rate inside the aluminium foam portion (aluminium foam fin) because of high flow resistance caused by the aluminium foam.

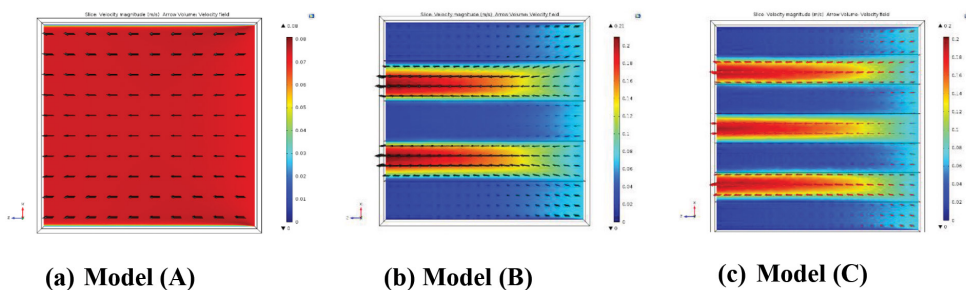


Figure 20. Velocity contours at $q''=13.8 \text{ W/cm}^2$, $Re=1353$

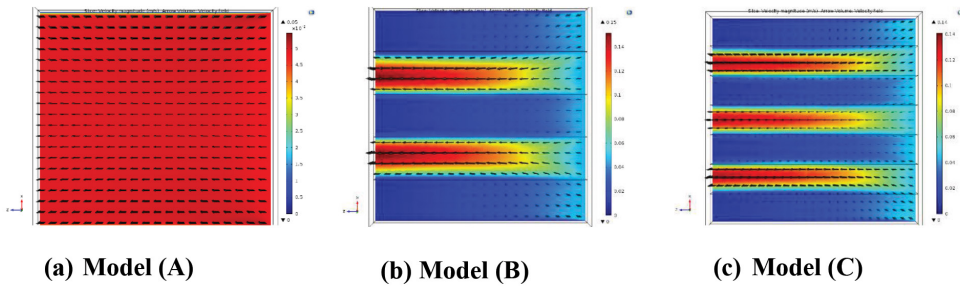


Figure 21. Velocity contours at $q'' = 13.8 \text{ W/cm}^2$, $Re=902$

Figure 22 shows the velocity profile at $Re=1353$ in order to provide a better picture of the velocity profiles of the models. The figure illustrates that model (A) achieved a perfect uniform flat velocity profile around 0.07 m/s . The figure also illustrates that models (B) and (C) achieved large parabolic velocity profiles through the channels and lower flat velocity profiles in aluminium foam portion. The same trend can be observed in Figure 23 at $Re=902$.

This means that due to the high flow resistance caused by the aluminium foam, around 70% of water flow goes into the empty channel and around 30% of the flow goes into the aluminium foam portion, which causes decreases in the positive effect of the aluminium foam on the heat transfer rate. The velocity profiles of models (B) and (C) also revealed that a larger percentage of the water flow entered the aluminium foam portion of model (B). That is why model (B) achieved a higher heat transfer rate than model (C).

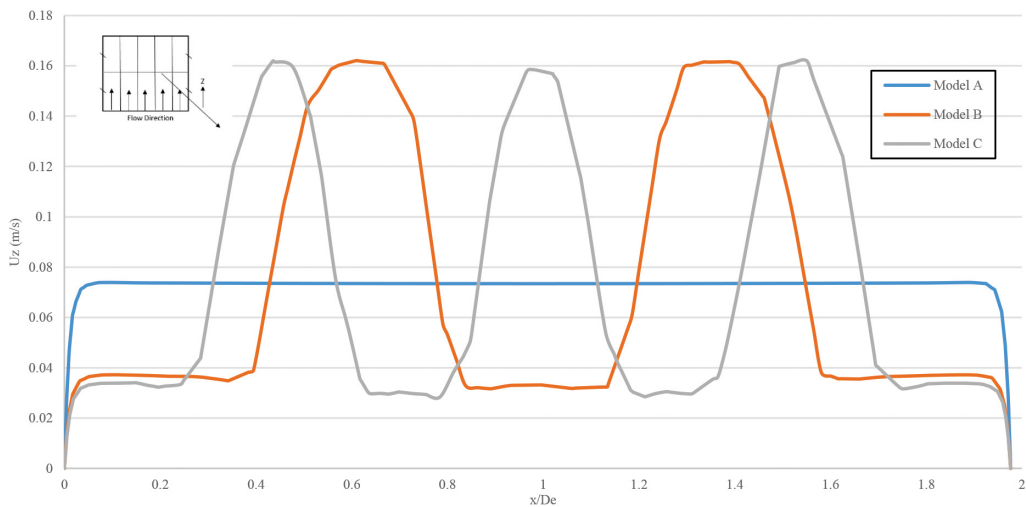


Figure 22. Velocity profile at $Re= 1353$

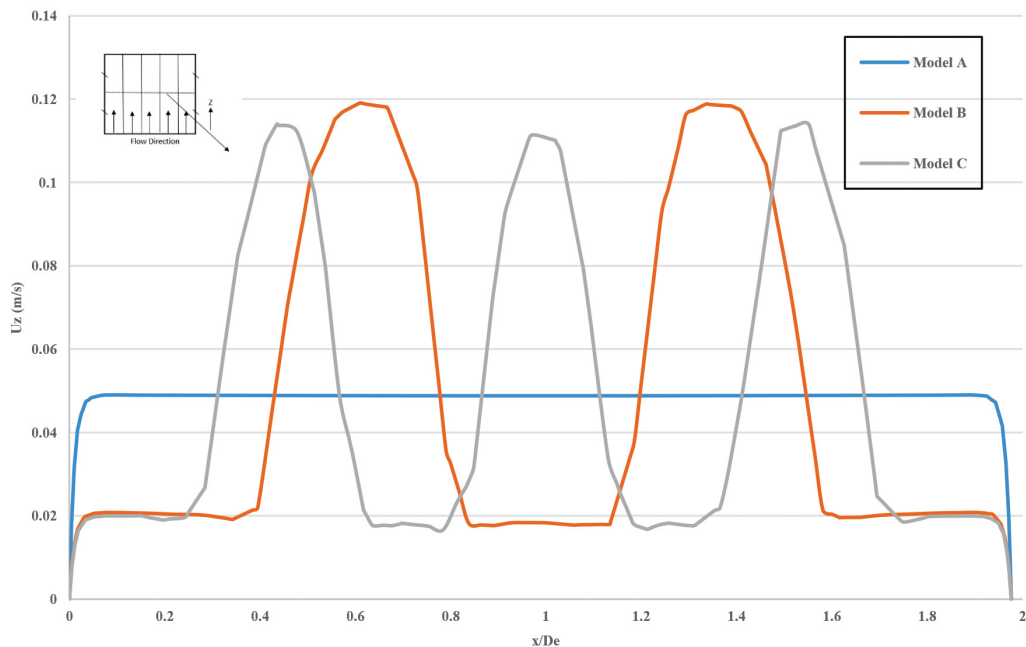


Figure 23. Velocity profile at $Re=902$

On the other hand, the results showed that the percentage of the flow which goes into the aluminium foam portion decreases along with the flow direction. This phenomenon occurs because the fluid particles turn from the aluminium foam portion (high flow resistance) to the empty channel. In order to take a closer look at this phenomenon, a particle tracing study was conducted using the finite element method. The results are displayed in Figure 24. As we can see, a portion of the fluid particles (red point) turn from the aluminium fin to the empty channel.

Thermal Performance of the Aluminium Foam Heat Sink Models

In order to evaluate the thermal performance of the aluminium foam heat sink models, the pressure drop across the aluminium foam was measured. Figure 25 illustrates the pressure drop versus the Reynolds number for models A, B and C. As we can see in this figure, the pressure drop increases along with increases in the Reynolds number and model (A) achieved a higher pressure drop than models (B) and (C). There was good agreement between the numerical and experimental pressure drop results.

The Fanning friction factor (f) is commonly used to provide information regarding the required pressure drop of the heat exchanger. This is done to ensure that the pressure drop across the foam is non-dimensional. The friction factor of aluminium foam is obtained using the following equation:

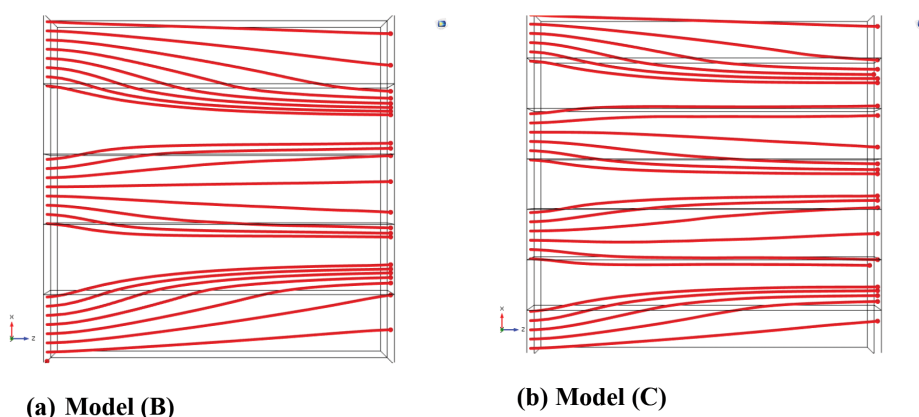


Figure 24. Fluid flow particle tracing at Re=1353

$$f_{friction} = \frac{\Delta p}{4\left(\frac{L}{De}\right)\left(\frac{\rho U^2}{2}\right)} \tag{18}$$

Where L represents the channel length, De represents the hydraulic diameter of the channel, ρ represents the water density, and U represents the velocity of the fluid. Figure 26 illustrates the friction factor of the foam verses the Reynolds number.

As we can see from the analysis of the heat transfer characteristics of water flow through the aluminium foam models, the average Nusselt number for all three models increased along with increases in the Reynolds number. This increase is accompanied by an increase in the required pumping power which is due to an increase in the pressure drop across the aluminium foam. In order to combine the heat transfer rate with the pressure drop, the thermal efficiency index is calculated using the following equation:

$$I_{efficiency} = \frac{Nu_{avg} * L}{f_{friction} * H} \tag{19}$$

Where $f_{friction}$ represents the Fanning friction factor of the aluminium foam, L represents the channel length, H represents the channel height, and Nu_{avg} represents the average Nusselt number. The thermal efficiency index combines the heat transfer with the pressure drop across the aluminium foam in order to find the optimal design condition that achieves higher heat transfer with lower pumping power. Figure 27 shows the thermal efficiency index verses the Reynolds number. As we can see in this figure, Model (B) achieved a higher thermal efficiency index over the Reynolds number range compared with models (A) and (C) based on the heat transfer rate and required pumping power. Model (B) achieved a thermal efficiency index of 6.1 at Re=1353, which represents the optimal design condition.

Heat Transfer Characteristics of AMF

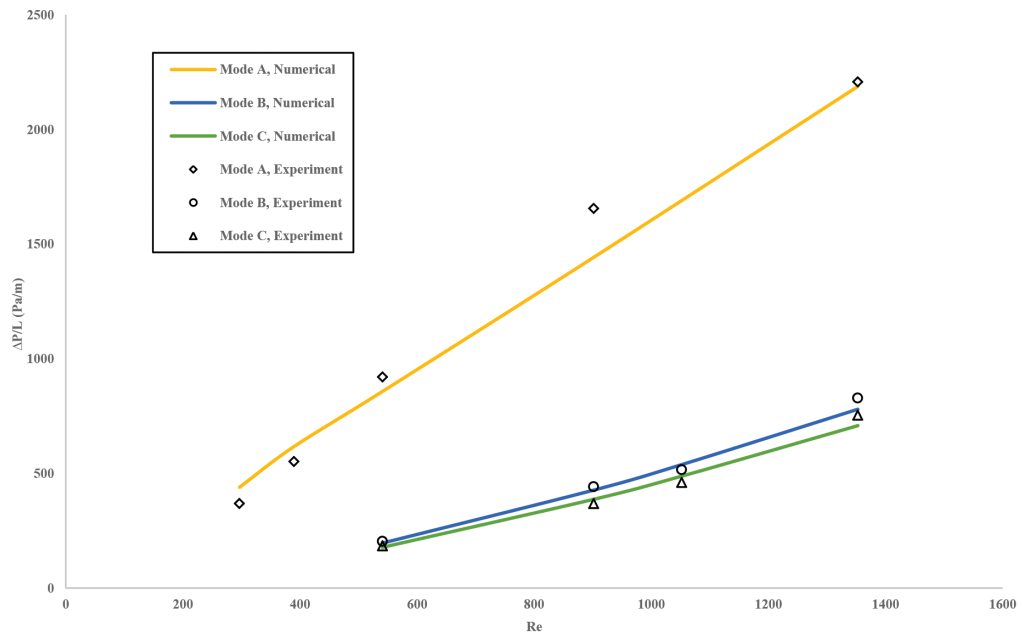


Figure 25. Pressure drop versus Reynolds number

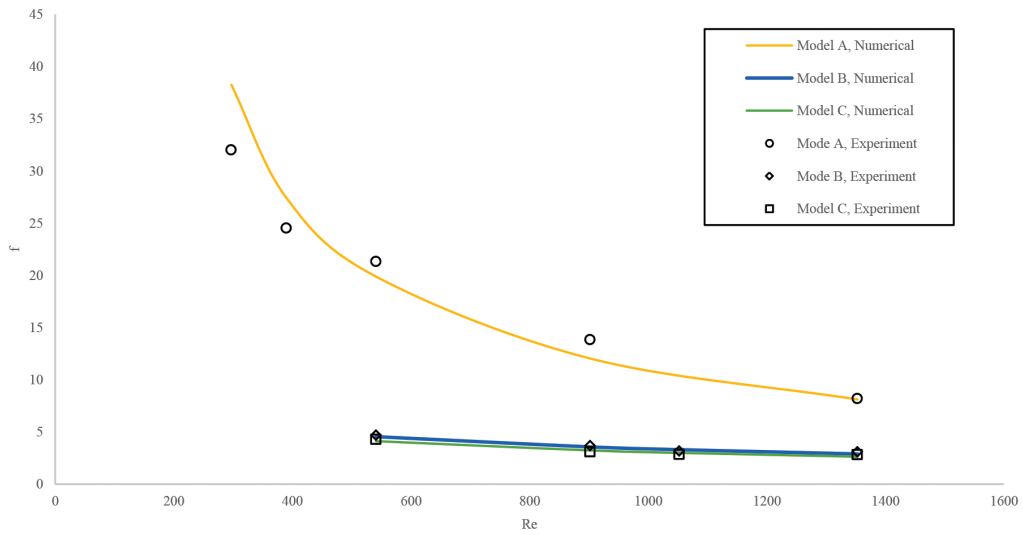


Figure 26. Fanning friction factor versus Reynolds number

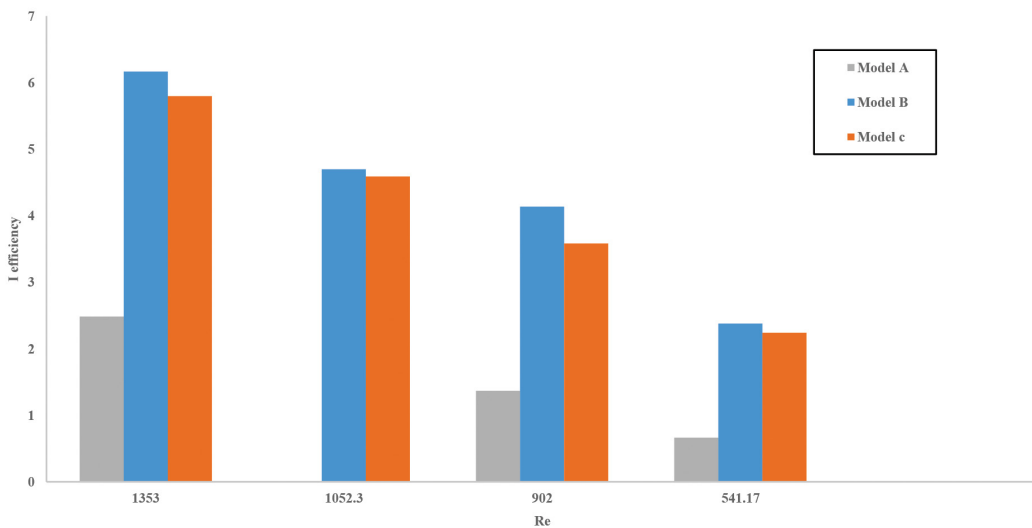


Figure 27. Thermal efficiency index versus Reynold number

CONCLUSIONS

This paper presents an experimental and numerical study of three different aluminium foam heat sink models in the cooling of an Intel core i7 processor (electronic cooling). The aluminium foam models were model (A) (without channels), model (B) with two channels and model (C) with three channels. The aluminium foam was subjected to a water flow covering the non-Darcy flow regime. The following conclusions were drawn based on the findings of the study:

- The local temperature distributions for models A, B and C increase along with increases in the dimensionless flow direction axis, decreasing the Reynolds number and increasing the heat flux.
- Model (A) achieved a lower local temperature than models (B) and (C).
- The numerical local surface temperature results were in good agreement with the experimental results, with a maximum relative error of 2%.
- At any given Reynolds number, the local Nusselt number is inversely proportional to the boundary layer thickness and reaches a constant value at the fully developed region.
- Model (A) achieved a higher local Nusselt number than model (B), and model (B) achieved a higher local Nusselt number than model (C).
- The numerical results of the local Nusselt number were in good agreement with the experimental results, with a maximum relative error of 3%.
- The average Nusselt number of models A, B and C increase along with increases in the Reynolds number.

- Models (B) and (C) reduced the average Nusselt number by 10% and 25% respectively, compared with model (A).
- The pressure drop across the foam was measured. The results revealed that the pressure drop increases as the Reynolds number increases.
- The pressure drop across model (A) was higher than the pressure drop across models (B) and (C).
- The thermal efficiency index combines heat transfer with the pressure drop across the aluminium foam models in order to find the optimal design condition that achieves higher heat transfer with lower pumping power. Model (B) achieved the optimal design condition with a thermal efficiency index of 6.1 at $Re = 1353$.

ACKNOWLEDGEMENTS

The authors acknowledge the full financial support of the National Science and Engineering Research Council (NSERC).

REFERENCES

- Bai, M., & Chung, J. (2011). Analytical and numerical prediction of heat transfer and pressure drop in open-cell metal foams. *International Journal of Thermal Sciences*, 50(6), 869-880.
- Bayomy, A., Saghir, M., & Yousefi, T. (2016). Electronic Cooling Using Water Flow in Aluminium Metal Foam Heat Sink: Experimental and Numerical Approach. *International Journal of Thermal Sciences*, 109, 182-200.
- Bhattacharya, A., & Mahajan, R. (2002). Finned metal foam heat sinks for electronics cooling in forced convection. *Journal of Electronic Packaging*, 124(3), 155-163.
- Boomsma, K., & Poulikakos, D. (2001). On the Effective Thermal Conductivity of a Three-Dimensionally Structured Fluid-Saturated Metal Foam. *International Journal of Heat Mass Transfer*, 44(4), 827-836.
- Boomsma, K., Poulikakos, D., & Zwick, F. (2003). Metal foams as compact high performance heat exchangers. *Mechanics of materials*, 35(12), 1161-1176.
- Buller, M., & Kilburn, R. (1981). Calculation of surface heat transfer coefficient for electronic module. *Heat Transfer in Electronic Equipment, HTD, ASME Winter Annual Meeting*, 20, 15-29
- Calmidi, V. V., & Mahajan, R. L. (2000). Forced Convection in High Porosity Metal Foams. *Journal of Heat Transfer*, 122(3), 557-565.
- Calmidi, V., & Mahajan, R. (1999). The effective thermal conductivity of high porosity fibrous metal foams. *Journal of Heat Transfer*, 121(2), 466-471.
- COMSOL Multiphysics. (2015, March). *COMSOL Multiphysics*. Retrieved from <http://www.comsol.com/comsol-multiphysics>
- Darcy, H. (1856). *Les Fontaines Publiques de la Ville de Dijon*. Victor Dalmont, Paris.

- Ding, X., Lu, L., Chen, C., He, Z., & Ou, D. (2011). Heat transfer enhancement by using four kinds of porous structures in a heat exchanger. In *Applied Mechanics and Materials* (Vol. 52, pp. 1632-1637). Trans Tech Publications.
- Dukhan, N., Bağcı, Ö., & Özdemir, M. (2015). Thermal development in open cell metal foam: an experiment with constant heat flux. *Journal of Heat and Mass Transfer*, 85, 852-859.
- Fu, H., Leong, K., Huang, X., & Liu, C. (2001). An experimental study of heat transfer of a porous channel subjected to oscillating flow. *Journal of heat transfer*, 123(1), 162-170.
- Gochman, S., Ronen, R., Anati, I., Berkovits, A., Kurts, T., Naveh, A., ... Valentine, R. C. (2003). The Intel Pentium M processor: microarchitecture and performance. *Intel Technology Journal*, 7(2), 21-36.
- Hetsroni, G., Gurevich, M., & Rozenblit, R. (2005). Metal foam heat sink for transmission window. *International journal of heat and mass transfer*, 48(18), 3793-3803.
- Hooman, K., & Ejlali, A. (2007). Entropy generation for forced convection in a porous saturated circular tube with uniform wall temperature. *International communications in heat and mass transfer*, 34(4), 408-419.
- Hwang, J., Hwang, G., Yeh, R., & Chao, C. (2002). Measurement of interstitial convective heat transfer and frictional drag for flow across metal foams. *Journal of Heat Transfer*, 124(1), 120-129.
- Igarashi, T., Nakamura, H., & Fukuoka, T. (2004). Pressure drop and heat transfer of arrays of in-line circular blocks on the wall of parallel channel. *International journal of heat and mass transfer*, 47(21), 4547-4557.
- Iwasaki, H., & Ishizuka, M. (2000). Forced convection air cooling characteristics of plate fins for notebook personal computers. In *The Seventh Intersociety Conference on Thermal and Thermomechanical Phenomena in Electronic Systems, 2000. ITherm 2000*. (Vol. 2, pp. 21-26). IEEE.
- Jubran, B., Swiety, S., & Hamdan, M. (1996). Convective heat transfer and pressure drop characteristics of various array configurations to simulate the cooling of electronic modules. *International Journal of Heat and Mass Transfer*, 39(16), 3519-3529.
- Kaviany, M. (1995). *Principles of Heat Transfer in Porous Media* (2en Ed.). Springer-Verlag, New York.
- Kim, S. Y., Paek, J. W., & Kang, B. H. (2003). Thermal Performance of aluminium foam heat sinks by forced air cooling. *IEEE transactions on components and packaging technologies*, 26(1), 262-267.
- Klett, J., Stinton, D., Ott, R., Walls, C., Smith, R., & Conway, B. (2001). *Heat exchangers/radiators utilizing graphite foams*. Oak Ridge National Laboratory, US Department of Energy.
- Lee, J. (2009). *Convection performance of nanofluids for electronics cooling*. (Doctoral Dissertation). Stanford University.
- Lu, W., Zhao, C., & Tassou, S. (2006). Thermal analysis on metal foam filled heat exchangers Part I: Metal-foam filled pipes. *International journal of heat and mass transfer*, 49(15), 2751-2761.
- Mancin, S., Zilio, C., Diani, A., & Rossetto, L. (2012). Experimental air heat transfer and pressure drop through copper foams. *Experimental thermal and fluid science*, 36, 224-232.
- Nield, D., Kuznetsov, A., & Xiong, M. (2003). Thermally developing forced convection in a porous medium: Parallel-plate channel or circular tube with walls at constant heat flux. *Journal of Porous Media*, 6(3), 203-212.

- Noh, J., Lee, K., & Lee, C. (2006). Pressure loss and forced convective heat transfer in an annulus filled with aluminium foam. *International communications in heat and mass transfer*, 33(4), 434-444.
- Rachedi, R., & Chikh, S. (2001). Enhancement of electronic cooling by insertion of foam materials. *Heat and Mass Transfer*, 37(4-5), 371-378.
- Seyf, H., & Layeghi, M. (2010). Numerical analysis of convective heat transfer from an elliptic pin fin heat sink with and without metal foam insert. *Journal of Heat Transfer*, 132(7), 1-9.
- Sparrow, E., Niethammer, J., & Chaboki, A. (1982). Heat transfer and pressure drop characteristics of array of rectangular modules in electronic equipment. *International Journal of Heat and Mass Transfer*, 25(7), 961-973.
- Sparrow, E., Yanezmoreno, A., & Otis, D. (1984). Convective heat transfer response to height differences in an array of block-like electronic components. *International journal of heat and mass transfer*, 27(3), 469-473.
- Sung, H., Kim, S., & Hyun, J. (1995). Forced convection from an isolated heat source in a channel with a porous medium. *International Journal of Heat and Fluid Flow*, 16(6), 527-535.
- Taylor, J. (1995). *An Introduction to Error Analysis-Study of Uncertainty in Physical Measurements*. Oxford University Press.
- Tzeng, S. C., Jeng, T. M., & Wang, Y. C. (2006). Experimental study of forced convection in asymmetrically heated sintered porous channel with/without periodic baffles. *International Journal of Heat and Mass Transfer*, 49(1), 78-88.
- Zhao, C., Kim, T., & Hodson, H. (2004). Thermal Transport in High Porosity Cellular Metal Foams. *Journal of Thermophysics and Heat Transfer*, 18(3), 309-317.
- Zhao, C., Lu, W., & Tassou, S. (2006). Thermal analysis on metal-foam filled heat exchangers. Part II: Tube heat exchangers. *International journal of heat and mass transfer*, 49(15), 2751-2761.
- Zhao, C. (2012). Review on thermal transport in high porosity cellular metal foams with open cells. *International Journal of Heat and Mass Transfer*, 55(13), 3618-3632.

NOMENCLATURE

q''	Heat flux (W/cm ²)		
Nu_x	Local Nusselt number	F	Body force (N)
Nu_{avg}	Average Nusselt number	D_e	Hydraulic diameter (m), $D_e = \frac{4 * \text{Cross section area}}{\text{Wetted perimeter}}$
Re	Reynolds number	T^*	Dimensionless temperature $\left[T^* = \frac{T - T_{in}}{q'' * \frac{D_e}{k_{eff}}} \right]$
U	Velocity fields (m/s)	x^*	Dimensionless flow direction axis, $x^* = \frac{x}{D_e}$
K_b	Permeability (m ²)	ΔP	Pressure difference (Pa)
k_f	Thermal conductivity of fluid	$I_{efficiency}$	Thermal efficiency index
d_f	Ligament diameter (m)	Greek symbols	
k_s	Thermal conductivity of solid (W/m.K)	ρ	Density (kg/m ³)
K_{eff}	Effective thermal conductivity (W/m.K)	C_p	Specific heat (J/kg.°C)
T_x	Local surface temperature (°C)	ε	Porosity
$f_{friction}$	Fanning friction factor	ν	Kinematic viscosity (m ² /s)
T_{in}	Inlet water bulk temperature (°C)	β_f	Forchheimer coefficient
h_x	Local heat transfer coefficient (W/m ² K)	μ	Dynamic viscosity (Pa. s)